Comprehensive Quantification of Height Dependence of Entrainment-Mixing between Stratiform Cloud Top and Environment

Sinan Gao[1], Chunsong Lu[1]*, Yangang Liu[2], Seong Soo Yum[3], Jiashan Zhu[1], Lei Zhu[1], Neel Desai[2a], Yongfeng Ma[4], Shang Wu[1]

[1]Collaborative Innovation Center on Forecast and Evaluation of Meteorological Disasters, Key Laboratory for Aerosol-Cloud-Precipitation of China Meteorological Administration, Nanjing University of Information Science & Technology, Nanjing, China

[2]Environmental and Climate Sciences Department, Brookhaven National Laboratory, Upton NY, US

[3]Department of Atmospheric Sciences, Yonsei University, Seoul, South Korea

[4]Department of Mechanics & Aerospace Engineering, Southern University of Science and Technology, Shenzhen, China

Correspondence to: Chunsong Lu (luchunsong110@gmail.com)

---

[a] Now at Department of Meteorology and Climate Science, San Jose State University, San Jose, CA

Abstract. Different entrainment-mixing processes of turbulence are crucial to processes related to clouds; however, only a few qualitative studies have been concentrated on the vertical distributions of entrainment-mixing mechanisms with low vertical resolutions. To quantitatively study vertical profiles of entrainment-mixing mechanisms with a high resolution, the stratiform clouds observed in the Physics of Stratocumulus Top (POST) project are examined. The unique sawtooth flight pattern allows for an examination of the vertical distributions of entrainment-mixing mechanisms with a 5 m vertical resolution. Relative standard deviation of volume mean radius divided by relative standard deviation of liquid water content is introduced to be a new estimation of microphysical homogeneous mixing degree, to overcome difficulties of determining the adiabatic microphysical properties required in existing measures. The vertical profile of this new measure indicates that entrainment-mixing mechanisms become more homogeneous with decreasing altitudes and are consistent with the dynamical measures of Damkohler number and transition scale number. Further analysis shows that the vertical variation of entrainment-mixing mechanisms with decreasing altitudes is due to the increases of turbulent dissipation rate in cloud and relative humidity in droplet-free air, and the decrease of size of droplet-free air. The results offer insights into the theoretical understanding and parameterizations of vertical variation of entrainment-mixing mechanisms.

1 Introduction

Clouds are identified to be a significant origin of uncertainties in climate research, because of poor simulations of clouds (Bony and Dufresne, 2005; Stephens, 2005; Zheng and Rosenfeld, 2015; Zhao and Garrett, 2015; Wang et al., 2019; Cess et al., 1989; Wang, 2015; Gao et al., 2016; Grabowski, 2006; Morrison, 2015). Entrainment-mixing processes of turbulence have been considered as significant factors for various processes related to clouds (Su et al., 1998; Lasher‑trapp et al., 2005; Hoffmann and Feingold, 2019; Xu et al., 2020; Hudson et al., 1997; Liu et al., 2002). Therefore, it is vital to figure out the nature of interaction between clouds and environment and their impacts on cloud droplet properties (Xue and Feingold, 2006). Entrainment-mixing processes are considered to occur primarily near the stratiform cloud top and entrainment-mixing around the stratiform cloud sides is negligible (Wood, 2012; Xu and Xue, 2015).

The question about how entrained air affects cloud microphysics has been debated for a long time. Several conceptual models have been established to study the different entrainment-mixing processes, e.g., entity-type entrainment-mixing (Telford, 1996; Telford and Chai, 1980), vertical circulation entrainment-mixing (Yeom et al., 2017; Yum et al., 2015; Wang et al., 2009) and homogeneous (HM)/inhomogeneous (IM) entrainment-mixing (Baker et al., 1980; Baker et al., 1984). The last one is the most used and studied. During the HM mixing, the time scale for droplets to evaporate completely is larger than the time scale for mixing between entrained air and cloudy air. All droplets are exposed to the same unsaturated state and evaporate concurrently. In this scenario, all droplets' sizes decrease simultaneously, and number concentration also decreases due to the dilution effect of entrained air. While in the IM mixing, mixing time scale is larger than evaporation time scale. Some droplets adjacent to entrained air would evaporate completely to saturate the air, while the other droplets are not affected by the entrainment. In this scenario, number concentration decreases but droplet size remains unchanged. Some observational studies support the extreme IM concept (Burnet and Brenguier, 2007; Lu et al., 2011; Freud et al., 2011; Pawlowska et al., 2000; Haman et al., 2007; Freud et al., 2008); while some others indicate that the HM mixing dominates (Gerber et al., 2008; Lu et al., 2013c; Burnet and Brenguier, 2007; Jensen et al., 1985), and still some others find intermediate features fall in between the HM and IM mixing (Lehmann et al., 2009; Lu et al., 2014a; Kumar et al., 2018).

The vertical variation of entrainment-mixing mechanisms is less studied. For cumulus, Small et al. (2013) and Jarecka et al. (2013) found that a trend existed of entrainment-mixing to be more HM in cloud top, resulted from increasing of cloud droplet radius and turbulence with increasing altitudes. In stratiform clouds, Yum et al. (2015) and Wang et al. (2009) observed positive correlation at middle of cloud and no correlation at cloud top between droplet size and liquid water content. Yum et al. (2015) suggested that entrainment mixing at cloud top region was indeed IM, while during the descent of vertical circulation, the cloud droplets in more diluted parcels would evaporate faster, and observe the generally HM feature at a relatively long depth

59   from cloud top.

60

61   The above few studies are largely qualitative and based on horizontal flight legs with coarse vertical resolutions. Furthermore,

62   these studies often need to determine adiabatic cloud microphysical properties from observational data, which are full of known

63   and unknown uncertainties (e.g., Jensen et al., 1985; Yum et al., 2015; Lu et al., 2014b; Yeom et al., 2017).

64

65   This study aims to overcome these limitations by examining the data from the field campaign of Physics of Stratocumulus Top

66   (POST) (Hill et al., 2010; Malinowski et al., 2010; Gerber et al., 2010) for the high-resolution vertical variation of entrainment-

67   mixing processes. Four measures of microphysical homogeneous mixing degrees (HMDs) that require the determination of

68   adiabatic cloud properties (Lu et al., 2014b; Lu et al., 2013b; Lu et al., 2014a) are examined and inconsistencies are discussed.

69   A new microphysical measure is proposed to quantify the entrainment-mixing mechanisms to overcome the drawbacks of the

70   existing methods that require cloud adiabatic properties. Physical reasons for the vertical variation of entrainment-mixing

71   mechanisms are analyzed using a comprehensive microphysical-dynamical approach.

72

73   The rest of this study is presented as follows. The POST dataset and the existing methods for calculating microphysical and

74   dynamical measures of HMD are presented in Section 2. Section 3 first shows the analysis of entrainment-mixing mechanisms

75   using the existing microphysical measures and dynamical measures. A new microphysical measure is then introduced to

76   represent entrainment-mixing mechanisms after discussing the potential uncertainties in choosing and determining the

77   adiabatic properties needed for the existing microphysical measures. The key factors affecting vertical variation of

78   entrainment-mixing are examined as well. Section 4 is the concluding remarks.

79   **2 Dataset and Methods**

80   **2.1 Dataset**

81   POST was designed to further the understanding of the physical processes around stratiform cloud top zone (Carman et al.,

82   2012; Gerber et al., 2010; Hill et al., 2010; Malinowski et al., 2010; Ma et al., 2017; Jen-La Plante et al., 2016; Ma et al., 2018;

83   Kumala et al., 2013). During POST campaign, thermodynamic, dynamical, and microphysical properties were measured on

84   board in July and August of 2008 with a total of 17 research flights. Flights were implemented in the vicinity of the coast of

85   Santa Cruz/Monterey, California, US, within $36°$ to $37°$N and$123°$ to $124°$W (Gerber et al., 2010; Hill et al., 2010; Malinowski

86   et al., 2010).

87

88   The Cloud and Aerosol Spectrometer (CAS) probe measured size distributions in the radius range of 0.29 - 25.5 μm at the

89   frequency of 10 Hz. The data in the radius range of 1.0 - 25.5 μm are used to calculate microphysical properties, i.e., number

90   concentration (n_c), liquid water content (LWC_c) and volume mean radius (r_{vc}). The Modified Ultrafast Thermometer (UFT-M)

91   was the temperature probe. Only the flights with good quality temperature data (no reports of "noise", "spike" or "holes in the

92   data" in the data description file) are used. Although the time resolution of temperature data was as high as 1000 Hz (Kumala

93   et al., 2013), 10 Hz data are used here. Humidity was measured by the EDGETECH EG&G Chilled Mirror at 10 Hz. For

94   turbulence measurements, the five-hole gust detector provided by University of California, Irvine (UCI) was used to collect

95   high resolution wind velocities at 40 Hz. We use 10 cm^{-3} of n_c and 0.001 g m^{-3} of LWC_c to be the standard of threshold values

96   to select cloudy samples (Lu et al., 2014b; Deng et al., 2009; Zhang et al., 2011). We define the cloud base as the lowest

97   altitudes where the samples satisfy the previously mentioned cloud criteria. We focus only on the non-drizzling clouds, and

98   the threshold value of drizzle water content in cloud using Cloud Imaging Probe (CIP) measurements (radius larger than 25

99   μm) is 0.005 g m^{-3} (Lu et al., 2011). A total of 4 flights in POST (July 16, August 02, 06, 08, 2008) satisfying the above criteria

100   is selected to examine the vertical variation of entrainment-mixing mechanisms.

101   **2.2 Sawtooth Pattern Flights**

102   Unlike most aircraft campaigns, the POST flights were designed as sawtooth legs to examine detailly the vertical structures of

103   the stratiform cloud top zone (Figure 1 (a)) (Carman et al., 2012; Gerber et al., 2013; Jen-La Plante et al., 2016). About 60

104   sawtooth legs are contained in each flight (Gerber et al., 2013; Carman et al., 2012). In this way, high-resolution vertical

105   profiles near cloud top can be obtained, which are not available from the conventional sampling along horizontal legs. Because

106   the cloud top altitudes vary spatially, we calculate the average cloud top altitude measured by each sawtooth profile and only

107   the sawtooth legs with cloud tops 30 m above/below the average cloud top are selected. The procedure of altitude stratification

108   is illustrated in Figure 1 (b). We take 5 m as the vertical interval of all sawtooth patterns. All the analyses below are based on

109   the cloud properties averaged over the 5 m vertical intervals and each vertical interval consists of thousands of data. Only the

110   height intervals over which the average droplet-free air sizes (i.e., non-cloudy sample sizes between cloudy samples) are larger

111   than zero are analyzed, which is detailed later in Figure 10. The results are similar when the vertical resolution of all sawtooth

112   patterns is set as 3 m and 7 m, respectively (not shown).

113   **2.3 Methods**

114   **2.3.1 Existing Microphysical Measures of Homogeneous Mixing Degree**

115   Based on the diagram of microphysical mixing, four HMDs have been defined to contain all kinds of entrainment mixing

116   mechanisms. The first three measures are based on the diagram of r_{vc}^3/r_{va}^3 versus n_c/n_a (Lu et al., 2014a; Lu et al., 2013b), as

117   shown in Figure 2 (a) and (b). Figure 2 (a) declares the various status during a whole process of entrainment-mixing for

118   defining the first measure (ψ_1). The adiabatic cloud is represented by Point A with the number concentration (n_a) and volume

119   mean radius (r_{va}) of adiabatic state. After environmental air is entrained into cloud, the state of cloud approaches Point B,

120   which number concentration is n_h and volume mean radius is r_{va}. Then mixing and evaporation processes occur and cloud state

121   approaches Point C, where number concentration after evaporation is n_c and volume mean radius after evaporation is r_{vc}. The

122   included angle between the line connecting Point B to Point E and the extreme IM mixing line is $\pi/2$, and the included angle

123   between the line connecting Point B to Point C and the extreme IM mixing line is β. Then ψ_1 is defined as:

124    $$\psi_1 = \frac{\beta}{\pi/2},$$ (1a)

125   where β is

126    $$\beta = \arctan(\frac{r_{vc}^3/r_{va}^3 - 1}{n_c/n_a - n_h/n_a});$$ (1b)

127    $n_h = n_a \times \chi$ and χ represents the adiabatic cloud fraction after mixing derived from energy conservation and total water

128   conservation in the isobaric mixing (Lehmann et al., 2009; Gerber et al., 2008; Lu et al., 2012). The second HMD (ψ_2) is

129   defined in view of Figure 1 (b):

130    $$\psi_2 = \frac{1}{2}(\frac{n_c - n_i}{n_h - n_i} + \frac{r_{vc}^3 - r_{va}^3}{r_{vh}^3 - r_{va}^3}),$$ (2)

131   where $n_i = \frac{r_{vc}^3}{r_{va}^3} n_c$ and   (3)

132    $$r_{vh}^3 = \frac{n_c}{n_h} r_{vc}^3.$$ (4)

133   Here n_i is the number concentration after extreme IM mixing and r_{vh} is the volume mean radius after HM mixing. The third

134   measure of HMD (ψ_3) is given by

135    $$\psi_3 = \frac{\ln(n_c) - \ln(n_i)}{\ln(n_h) - \ln(n_i)} = \frac{\ln(r_{vc}^3) - \ln(r_{va}^3)}{\ln(r_{vh}^3) - \ln(r_{va}^3)}.$$ (5)

136   The fourth measure (ψ_4) is defined using mixing diagram of r_{vc}^3/r_{va}^3 versus LWC_c/LWC_a (Lu et al., 2014b), as shown in Figure

137   2 (c),

138    $$\psi_4 = \frac{1 - r_{vc}^3/r_{va}^3}{1 - LWC_c/(\chi LWC_a)}.$$ (6)

139   The meanings of the Points A - E are the same as those in Figures 2 (a) and 2 (b). Four kinds of HMDs are expected to range

140 from 0 to 1, the higher probability of HM mixing corresponds to the larger HMD value.

141

142 A new dimensionless HMD (ψ_5) is introduced to quantify the different entrainment-mixing mechanisms:

143 $$\psi_5 = dis(r_{vc}^{3}) / dis(\text{LWC}_c), \tag{7}$$

144 where dis represents the relative standard deviation expressed by the ratio of standard deviation to the average value over each

145 level. During entrainment-mixing and evaporation processes, LWC_c always decreases but r_{vc} decreases in the HM mixing and

146 remains constant in the extreme IM mixing. Therefore, the extreme IM mixing corresponds to $\psi_5 = 0$, and the larger the value

147 of ψ_5 is, the more HM the entrainment mixing is. More discussions on ψ_5 are given in Section 3.2.

2.3.2 Dynamical Measures of Homogeneous Mixing Degree

149 The dynamical aspect, i.e., the mixing process between cloud and environment air *vs*. the evaporation process of cloud droplets,

150 is important to distinguish different entrainment-mixing mechanisms (Baker et al., 1980; Baker and Latham, 1979). The mixing

151 time scale divided by evaporation time scale is defined as Damkohler number (Da), which is usually used to quantify mixing

152 process is faster or evaporation process is faster and thus to discern the entrainment-mixing mechanisms (Siebert et al., 2006;

153 Burnet and Brenguier, 2007; Andrejczuk et al., 2009),

154 $$Da = \frac{\tau_{\text{mix}}}{\tau_{\text{r}}}, \tag{8}$$

155 where τ_{mix} and τ_{r} are turbulent mixing time and microphysical response time of droplets, respectively (Lehmann et al., 2009).

156 A more IM mixing corresponds to a larger Da. Three kinds of microphysical time scales, phase relaxation time (τ_{phase}) (Kumar

157 et al., 2013; Kumar et al., 2012), evaporation time (τ_{evap}) (Andrejczuk et al., 2009; Baker et al., 1980; Burnet and Brenguier,

158 2007), and reaction time (τ_{react}) (Lehmann et al., 2009; Lu et al., 2011; Lu et al., 2013c; Lu et al., 2014b), have been used to

159 represent τ_{r}. Lu et al. (2018) found that the most appropriate time scale was τ_{evap} if we focus on the changes of number

160 concentration and radius of droplets. The mixing time scale is defined as follows:

161 $$\tau_{\text{mix}} \sim (L^3 / \varepsilon)^{1/3}, \tag{9}$$

162 where ε is the turbulent dissipation rate calculated from the three dimensional wind velocities (Meischner et al., 2001) (see

163 Appendix A for details), and L is the size of droplet-free air calculated with

164 $$L = F \times TAS/f, \tag{10}$$

165 where droplet-free sample size divided by the sum of cloud and droplet-free sample size is considered as fraction of droplet-

166 free F in each vertical interval (e.g., if there are 90 cloud samples and 10 non-cloudy samples, $F = 10/(10+90) = 10\%$); TAS

167 and f are the aircraft true air speed (~ 55 m s^{-1}) and sampling frequency (10 Hz), respectively. The size of droplet-free air is

168 used as a proxy for the entrained air parcels' size. In equation (8), the time scale for a droplet of radius r_{va} to completely

169 evaporate (evaporate time) is given by:

170
$$\tau_{\text{evap}} = -\frac{r_{va}^2}{2AS_0},\tag{11}$$

171 where S_0 is the supersaturation of the droplet-free air at the corresponding altitude (Yau and Rogers, 1996); A is a affected by

172 air temperature and pressure (see Appendix B for details).

173

174 Another dynamical measure given by the ratio of L^* to η is transition scale number (N_L) (Lu et al. (2011)):

175
$$N_L = \frac{L^*}{\eta},\tag{12}$$

176 where transition length (L^*) is considered as the corresponding L value when $Da = 1$ (Lehmann et al., 2009) and is given as

177 follows:

178
$$L^* = \varepsilon^{1/2}\tau_r^{3/2}.\tag{13}$$

179 In equation (12), η is the Kolmogorov length scale (Wyngaard, 2010), which is given by:

180
$$\eta = (\frac{v^3}{\varepsilon})^{1/4},\tag{14}$$

181 where v is the kinematic viscosity (Wyngaard, 2010). A higher probability of HM mixing corresponds to a larger value of N_L.

182 **3 Results**

183 **3.1 Entrainment-Mixing Mechanisms from the Microphysical and Dynamical Perspectives**

184 It has been known that it can be uncertain and even problematic to determine the representative adiabatic values from the

185 observational data needed in calculation of the above-mentioned microphysical measures (Yeom et al., 2017; Jensen et al.,

186 1985; Yum et al., 2015). For example, because vertical velocity and concentration of cloud condensation nuclei can change

187 spatially in clouds, n_a and r_{va} change accordingly. Entrainment-mixing in clouds adds difficulties to determine accurate values

188 of r_{va}, n_a and LWC$_a$. Improper estimation of adiabatic values may violate the theoretical expectation: $n_a \geq n_h \geq n_c \geq n_i$ and $r_{va} \geq$

189 r_v, and then cause unrealistic HMDs. Different adiabatic variables have been used in previous studies. For example, the

190 maximum volume mean radius and number concentration are used as proxy values for r_{va} and n_a for each horizontal penetration,

191 respectively (Yeom et al., 2017; Yum et al., 2015); LWC$_a$ is calculated from the adiabatic growth from cloud base, and the

192   maximum number concentration of whole flight penetration is considered as n_a (Burnet and Brenguier, 2007; Lehmann et al.,

193   2009); n_a is the mean value of top 2% of n_c for each flight and r_{va} is calculated using adiabatic water vapor mixing ratio,

194   adiabatic total water mixing ratio and n_a for a horizontal penetration (Small et al., 2013).

195

196   To examine the influence of using different adiabatic properties, we compare ψ_i (i = 1 - 4) calculated with different adiabatic

197   variables (Table 1) at each level near the stratiform cloud tops for the data collected during the four flights. Only the results

198   for the first microphysical measure are shown in Figure 3; the other results are shown in the Supporting Information. In Figure

199   3, LWC_a is based on the adiabatic growth from cloud base, the maximum number concentration at each level is assumed as n_a,

200   and r_{va} is calculated from LWC_a and n_a. In Figure S1, LWC_a is based on the adiabatic growth from cloud base, the maximum

201   volume mean radius at each level is assumed as r_{va}, and n_a is calculated from LWC_a and r_{va}. In Figure S2, the maximum liquid

202   water content at each level is assumed as LWC_a, the maximum number concentration at each level is assumed as n_a, and r_{va} is

203   calculated from LWC_a and n_a. In Figure S3, the maximum liquid water content at each level is assumed as LWC_a, the maximum

204   volume mean radius at each level is assumed as r_{va}, and n_a is calculated from LWC_a and r_{va}. In Figure S4, the maximum number

205   concentration at each level is assumed as n_a, the maximum volume mean radius at each level is assumed as r_{va}, and LWC_a is

206   calculated from n_a and r_{va}. According to the definitions, ψ_i (i = 1 - 4) are expected to range from 0 to 1. However, some values

207   of ψ_i (i = 1 - 4) are larger than 1 or smaller than 0 in Figure 3 and Figures S1 – S4, which could be caused by uncertainties in

208   r_{va}, LWC_a, n_a and cloud base (Lu et al., 2014b; Lu et al., 2014a; Lu et al., 2013b; Gerber et al., 2008). Furthermore, these

209   figures suggest different vertical distributions of HMDs for the same flight, suggesting that high sensitivity of the conventional

210   HMDs to the methods for determining the adiabatic values could pose a serious problem as to which figure represents the

211   reality of entrainment-mixing mechanisms.

212

213   Since the above analysis from the microphysical perspective does not tell a consistent story about the vertical variation of

214   HMD, Da and N_L are examined from the dynamical perspective. Figures 4 (a), (c), (e) and (g) show the height dependence of

215   Da during each of the four flights. It is obvious that Da decreases with decreasing altitudes. Figures 4 (b), (d), (f) and (h) show

216   a significant increasing trend of N_L with decreasing altitudes. The method for setting the adiabatic values in Figure 4 is the

217   same as that in Figure 3, i.e., LWC_a is based on the adiabatic growth from cloud base, the maximum number concentration at

218   each level is assumed as n_a, and r_{va} is calculated from LWC_a and n_a. Unlike the microphysical measures, vertical variation of

219   Da or N_L are similar when different methods for determining adiabatic values are used (Figures S5 – S8). It is expected that a

220   smaller Da (larger N_L) represents a larger HMD. The results of Da and N_L both suggest more IM mixing closer to cloud top.

221   It is noteworthy that this result is robust, not affected by the methods for obtaining the adiabatic values, and thus should reflect

222   the real height dependence of entrainment-mixing mechanisms.

223

224   The different vertical distributions of HMDs and the inconsistency between microphysical HMDs and dynamical measures are

225   mainly due to the improper estimations of adiabatic values. For example, during the flight of 16 July in Figure 3, the HMDs

226   decrease with the decreasing altitudes, and most of the HMDs are negative. The negative values do not meet the theoretical

227   expectations and these trends are completely inconsistent with those of dynamical measures. The vertical variations of some

228   important properties of this case are shown in Figure 5. The negative values of HMDs are due to unexpected result of $r_{va} \leq r_{vc}$.

229   Under these circumstances, the difference between r_{vc} and r_{va} becomes larger with the decreasing altitudes, corresponding to

230   the decreasing trends of HMDs with the decreasing altitudes. Besides the first method, the other four methods mentioned above

231   also have their own unreasonable points. For example, $r_{va} \leq r_{vc}$ exists under the methods 1, 3 and 4; $n_a \leq n_c$ exists under the

232   methods 2 and 4; r_{va} does not always increase with the increasing altitudes under the methods 2, 4 and 5 (See figures S9 to

233   S13 for details). Overall, the inconsistency among the microphysical HMDs estimated with different methods to determine the

234   adiabatic variables calls for a new microphysical measure of entrainment-mixing mechanisms.

235   **3.2 New Microphysical Measure**

236   As discussed in Section 3.1, the existing microphysical measures of HMDs depend on the different adiabatic values to a great

237   extent. In order to avoid this kind of uncertainty, a new dimensionless HMD (ψ_5) in equation (7) is introduced to quantify the

238   different entrainment-mixing mechanisms. To make sure that ψ_5 is applied properly, the correlation between r_{vc}^3 and LWC_c

239   must be positive. If the correlation is negative, IM mixing with subsequent ascent is likely to occur (Lu et al., 2013a; Lehmann

240   et al., 2009; Wang et al., 2009; Siebert et al., 2006; Lasher‑trapp et al., 2005). It is worth mentioning that ψ_5 does not require

241   using adiabatic values, and thus can overcome the deficiencies of ψ_i (i = 1 - 4) associated with choosing different adiabatic

242   cloud properties.

243

244   The vertical variation of ψ_5 for the 4 flights are shown in Figure 6. The small value of ψ_5 near the cloud tops shows that

245   entrainment-mixing approaches extreme IM, consistent with conclusions in several previous studies based on the POST data

246   (Gerber et al., 2013; Gerber et al., 2016; Malinowski et al., 2013). The increase of ψ_5 with decreasing altitudes indicates that

247   the trends towards more HM with the decreasing altitudes, consistent with the results of Da and N_L (Figure 4 and Figures S5

248   – S8). We also check the relationship between r_{vc}^3 and LWC_c and the two quantities are positively correlated (not shown).

249

250   The relationships between ψ_5 versus Da and N_L of the 4 flights are shown in Figure 7 and are well fitted by the equations used

251   in Luo et al. (2020)

252    $$\psi_5 = a_1 \exp(b_1 Da^{c_1}), \tag{15}$$

253    $\psi_5 = a_2 \exp(b_2 N_L{}^{c_2})$,   (16)

254   where the parameters a_1 and a_2 are positive; b_1 and b_2 are negative; c_1 is positive and c_2 is negative. The negative correlation

255   of ψ_5 vs Da and positive correlation of ψ_5 vs N_L are evident and in keeping with theoretical arguments, suggesting that a smaller

256   Da or a larger N_L corresponds to a higher ψ_5. Such relationships further confirm the utility and applicability of ψ_5 in studying

257   entrainment-mixing mechanisms. The correlation coefficients of the linear regression of for ψ_5 vs Da and ψ_5 vs N_L are about

258   0.66 and 0.60, respectively, suggesting that Da and N_L are basically equivalent for understanding the entrainment-mixing

259   parameterization.

260

261   The equivalence of Da and N_L is further supported by the tight negative correlation between Da and N_L (Figure 8). Similar

262   results have been reported in Gao et al. (2018) using numerical simulations, and Desai et al. (2021) based on holographic

263   measurements. However, the underlying reasons are different. Figure 9 shows that L and L^* are negatively correlated, opposite

264   to the positive correlation between L^* and the Taylor microscale in Gao et al. (2018); Taylor microscale is used as L in the

265   calculation of τ_{mix} in equation (9) in Gao et al. (2018). It is easy to derive from equations (8), (9), (11) and (12) that $Da : N_L =$

266    $L : L^*$, others being equal:

267    $$\frac{Da}{N_L} = \frac{-2AS_0\eta}{\varepsilon^{1/3}r_{va}{}^2} \cdot \frac{L}{L^*}$$ (17)

268   Therefore, as long as L and L^* are nearly linearly correlated, Da and N_L are equivalent. When extreme IM mixing dominates

269   near cloud top, ε is small (Figure 10), which mainly determines small L^*; L is large near cloud top (Figure 10). Therefore, L

270   and L^* are negatively correlated. The vertical distributions of affecting factors on entrainment-mixing are detailed in the next

271   sub-section.

272

273   **3.3 Further analysis of Affecting Factors**

274   According to the analyses in Sections 3.1 and 3.2, the dynamical and microphysical measures both indicate that entrainment-

275   mixing mechanisms change from IM to HM with decreasing altitudes. Here we provide the physical explanation for such

276   behavior under the framework of HM/IM entrainment-mixing mechanisms, by analyzing the vertical variations of all the

277   variables defining Da and N_L, i.e., ε, relative humidity (RH) and L.

278

279   First, Figures 10 (a), (d), (g) and (j) show that ε increases with decreasing altitudes, which is opposite to that for cumulus

280   clouds (Small et al. (2013) and Jarecka et al. (2013)). According to definition of Da (equation (8)) and N_L (equation (12)), the

281   increase of ε leads to the decrease of Da and increase of N_L, others being equal. Therefore, ε is an important factor to cause Da

to decrease and N_{L} to increase with the decreasing altitudes (Figure 4 and Figures S5 – S8). The clouds were sampled in the vicinity of the coast of Santa Cruz/Monterey, California, therefore, these clouds were well-mixed and coupled, which explains the monotonic decrease of ε with the increasing height (Jones et al., 2011; Shupe et al., 2013). Note that the decoupled clouds should be very common in the downstream regions (Bretherton and Wyant, 1997) and midlatitudes (Zheng et al., 2020). The boundary layer decoupling causes a decrease of turbulent kinetic energy near the cloud base, leading to a local minimum near the cloud base and a maximum in the middle of cloud layer which can be used to infer the profile of ε (Stevens, 2000). This is also demonstrated in the observations by Zheng et al. (2016) who found a significant role of decoupling in weakening the cloud-base updrafts. Therefore, in the future studies of decoupled stratocumulus in other regions, the results about entrainment-mixing mechanisms could be different due to the non-monotonic vertical variation of ε.

Second, the vertical variation of entrainment-mixing can also be attributed to that of entrained air sizes. Figures 10 (b), (e), (h) and (k) show that L decreases significantly with decreasing altitudes, which leads to a decrease of Da with decreasing altitudes since Da is proportional to τ_{mix}, and thus L. The importance of L has rarely been studied in previous literatures for height dependence of entrainment-mixing. The decrease of L with decreasing altitudes agrees generally with the cascade of breakdown of dry air parcels entrained at the cloud top.

Third, vertical variation of entrained air RH plays a significant part in determining the entrainment-mixing mechanisms. In former literatures (Yeom et al., 2017; Lu et al., 2018), RH is commonly assumed to be constant across multiple different altitudes when calculating τ_{evap} using $S_0 = $ RH - 1. In fact, RH should not be a constant. We determine RH as the mean RH of droplet-free air in each level. Figures 10 (c), (f), (i) and (l) show that RH increases with decreasing altitudes due to droplet evaporation. According to the definition of Da, Da decreases with the increase of τ_{evap}, and thus decreases with the increase of RH (equation (7) and (10)). Equations (10), (11) and (12) show that N_{L} increases with increasing RH. Both Da and N_{L} indicate more HM mixing at a lower altitude. These results suggest that the increases of ε and RH and the decrease of L with decreasing altitudes are in keeping with the variation of entrainment-mixing processes, together playing the primary role in determining the vertical distribution of HMD observed.

It is noted that, r_{va} also affects Da and N_{L} through its effect on τ_{evap}. However, r_{va} depends on how adiabatic values are estimated in Section 3.1 (Figure S9 – S14 in the Supporting Information). Therefore, the vertical variation of r_{va} is not analyzed here. No matter which method is used to determine the adiabatic values, the trends of vertical variation of Da and N_{L} do not change (Section 3.1). The vertical variation of Da and N_{L} indicates the dominance of the combined effects of ε, RH and L in determining the vertical variation of entrainment-mixing processes from IM towards HM with decreasing altitudes.

314 These results are in keeping with the results drawn in Wang et al. (2009) and Yum et al. (2015) in the sense that a trait of IM

315 mixing is prevalent near cloud top but at mid-levels of clouds a trait of HM mixing becomes dominant, according to the

316 analysis of cloud microphysical relationships at different altitudes of marine stratiform clouds. However, there are big

317 differences in the spatial scale of analysis between our and their studies. We focus on near cloud top regions from cloud top to

318 where droplet-free air patches can still be found, mostly less than 100 m from cloud top (Figure 3). On the other hand, Yum et

319 al. (2015) and Wang et al. (2009) examined mid-levels of stratiform clouds where there remained no droplet-free air patches

320 as well as near cloud top regions. They suggested that the vertical variation of cloud microphysical properties relationships

321 could be caused by vertical circulation of diluted parcels affected by entrainment; the actual mixing near cloud top might have

322 been IM as Da and N_L at this level suggested; as these parcels moved down, the droplets evaporated fast, resulting in cloud

323 microphysical relationships that would be explained as a trait of HM mixing.

324 **4 Concluding Remarks**

325 The observational data of marine stratiform clouds measured from aircraft during the campaign of Physics of Stratocumulus

326 Top (POST) are used to examine the height dependence of entrainment-mixing mechanisms. The sawtooth penetrations are

327 analyzed to acquire fine information on the vertical structure of entrainment-mixing near stratiform cloud tops, from the

328 microphysical and dynamical perspectives. To ensure high vertical resolution, we take 5 m as one altitude distance bin of all

329 sawtooth patterns for the four flights selected in this study.

330

331 From the microphysical perspective, the traditional homogeneous mixing degrees vary distinctly with the decreasing altitudes

332 due to different methods for obtaining adiabatic values. In order to overcome this difficulty, a new homogeneous mixing degree

333 describing the distributions of scatters in the mixing diagram is introduced to quantify different entrainment-mixing

334 mechanisms. The new homogeneous mixing degree is introduced by relative standard deviation of cubic volume mean radius

335 divided by relative standard deviation of liquid water content. If the new homogeneous mixing degree is larger, the mixing is

336 more likely to be homogeneous. The new measure increases with the decreasing altitudes, i.e., more homogeneous with

337 decreasing altitudes. This new measure is not affected by the methods for obtaining adiabatic values and shed new light on the

338 study of entrainment-mixing mechanisms.

339

340 From the dynamical perspective, Damkohler number decreases and transition scale number increases with decreasing altitudes.

341 The relationships between the new homogeneous mixing degree *vs*. Damkohler number and transition scale number are

342 negative and positive, respectively, consistent with theoretical expectation. Therefore, both microphysical and dynamical

343 analyses indicate the trends from inhomogeneous mixing to homogeneous mixing when altitude decreases.

344

345 The factors underlying the vertical variation of entrainment-mixing mechanisms are examined, including vertical distributions

346 of dissipation rate, size of droplet-free air and relative humidity in droplet-free air. Dissipation rate increases and droplet-free

347 air size decreases with the decreasing altitudes. Therefore, mixing is faster at the lower altitude and homogeneous mixing is

348 more likely to occur. Relative humidity increases with decreasing altitudes, which indicates that droplets are less likely to be

349 completely evaporated at the lower altitude. The combined effects of the three factors determine the entrainment-mixing

350 vertical evolution.

351

352 It is noteworthy that the traditional homogeneous mixing degrees are still useful properties to quantify entrainment-mixing

353 mechanisms, if adiabatic values of microphysical properties are properly determined. The new homogeneous mixing degree

354 defined here is a relative measure of homogeneous mixing degree as deviation from the extremely inhomogeneous mixing line,

355 but does not quantify the amount of homogeneous mixing precisely. The relative dispersion of volume-mean radius and liquid

356 water content increases due to differences in mixing states (Khain et al., 2018) and in-cloud activation of cloud condensation

357 nuclei (Derksen et al., 2009; Khain et al., 2018), which affects the calculation of the new homogeneous mixing degree. As

358 pointed out by Khain et al. (2018), the mixing diagram has limitations to analyze entrainment-mixing mechanisms using in

359 situ observations, due to transient mixing states. However, this new measure still provides an alternative method to quantify

360 entrainment-mixing mechanisms, supported by the independent Damkohler and transition scale numbers. This new method

361 can be applied to other datasets with different cloud droplet size probes (e.g., the Forward Scattering Spectrometer Probe,

362 FSSP), since the new definition is based on theoretical understanding of entrainment-mixing mechanisms, which is not limited

363 to the dataset used here. It would be interesting to apply this method to other stratocumulus and cumulus observations in

364 different climate zones.

365

366 **Code and Data Availability**

367 The codes can be accessed by contacting Chunsong Lu via luchunsong110@gmail.com. The POST data is available on

368 https://archive.eol.ucar.edu/projects/post/.

369

370 **Author Contributions**

371 SG performed the data analysis and manuscript writing. CL proposed the idea, guided this work and modified the

372 manuscript. YL and SSY supervised this work and helped revise the manuscript. JZ and LZ offered helps to the data

373   analysis. ND, YM and SW also contributed to the modification of manuscript.

374

375   **Competing Interests**

376   The authors declare that they have no conflict of interest.

377

378   **Appendix A**

379   Turbulent dissipation rate (ε) is calculated by three dimensional wind velocities (Meischner et al., 2001)

380    $$\varepsilon \approx \frac{D_{\mathrm{NN}}^{3/2}}{(4.01m)^{3/2}d},$$

381   (A1)

382   with $m \approx 0.2(2\pi)^{2/3}$ (Panofsky, 1984). D_{NN} is the local spatial structure function using three wind components and is defined as:

383    $$D_{\mathrm{NN}}(t,d) = \frac{1}{3}\{\frac{8}{7}[u(t)-u(t-\frac{d}{\mathrm{TAS}})]^2 + \frac{8}{7}[v(t)-v(t-\frac{d}{\mathrm{TAS}})]^2 + [w(t)-w(t-\frac{d}{\mathrm{TAS}})]^2\},$$ (A2)

384   where three wind components, east, north and vertical, are represented by u, v and w, respectively; TAS is the aircraft true air

385   speed ($\sim$55m s^{-1}); t is the time; d is the scale parameter:

386    $$d = \mathrm{TAS}\Delta t.$$ (A3)

387   where Δt is the time interval, which is set to 0.1 s.

388

389 **Appendix B**

390 The parameter A in equation (10) is

$$A = \frac{1}{[(\frac{L_h}{R_v T} - 1)\frac{L_h \rho_L}{KT} + \frac{\rho_L R_v T}{De_s(T)}]} \quad , \qquad (B1)$$

392 where R_v, L_h, T, K, ρ_L, D, and $e_s(T)$ are water vapor specific gas constant, latent heat, temperature, coefficient of air thermal

393 conductivity coefficient, liquid water density, water vapor diffusion coefficient in air and vapor pressure of saturation,

394 respectively.

395

Acknowledgment

The authors thank the crew of the POST campaign. This research was supported by the National Key Research and Development Program of China (2019YFA0606803), the Second Tibetan Plateau Scientific Expedition and Research (STEP) program (2019QZKK0105), the National Natural Science Foundation of China (41822504, 42027804, 42075073, 41975181), the Innovative Project of Postgraduates in Jiangsu Province in 2020 of Jiangsu (KYCX20_0933) and the China Scholarship Council. Y. Liu and N. Desai are supported by the U. S. Department of Energy Atmospheric System Research (ASR) program (DE-SC00112704); Y. Liu is also supported by Solar Energy Technologies Office (SETO) under Award 33504.

References

Andrejczuk, M., Grabowski, W. W., Malinowski, S. P., and Smolarkiewicz, P. K.: Numerical Simulation of Cloud–Clear Air Interfacial Mixing: Homogeneous versus Inhomogeneous Mixing, Journal of the Atmospheric Sciences, 66, 2493-2500, 10.1175/2009jas2956.1, 2009.

Baker, M., and Latham, J.: The evolution of droplet spectra and the rate of production of embryonic raindrops in small cumulus clouds, Journal of the Atmospheric Sciences, 36, 1612-1615, 1979.

Baker, M., Corbin, R., and Latham, J.: The influence of entrainment on the evolution of cloud droplet spectra: I. A model of inhomogeneous mixing, Quarterly Journal of the Royal Meteorological Society, 106, 581-598, 10.1002/qj.49710644914, 1980.

Baker, M., Breidenthal, R., Choularton, T., and Latham, J.: The effects of turbulent mixing in clouds, Journal of the atmospheric sciences, 41, 299-304, 10.1175/1520-0469(1984)041<0299:TEOTMI>2.0.CO;2, 1984.

Bony, S., and Dufresne, J. L.: Marine boundary layer clouds at the heart of tropical cloud feedback uncertainties in climate models, Geophysical Research Letters, 32, 10.1029/2005GL023851, 2005.

Bretherton, C. S., and Wyant, M. C.: Moisture transport, lower-tropospheric stability, and decoupling of cloud-topped boundary layers, Journal of Atmospheric Sciences, 54, 148-167, 1997.

Burnet, F., and Brenguier, J.-L.: Observational study of the entrainment-mixing process in warm convective clouds, Journal of the atmospheric sciences, 64, 1995-2011, 10.1175/JAS3928.1, 2007.

Carman, J., Rossiter, D., Khelif, D., Jonsson, H., Faloona, I., and Chuang, P.: Observational constraints on entrainment and the entrainment interface layer in stratocumulus, Atmospheric Chemistry and Physics, 12, 11135-11152, 2012.

Cess, R. D., Potter, G., Blanchet, J., Boer, G., Ghan, S., Kiehl, J., Le Treut, H., Li, Z.-X., Liang, X.-Z., and Mitchell, J.: Interpretation of cloud-climate feedback as produced by 14 atmospheric general circulation models, Science, 245, 513-516, 10.1126/science.245.4917.513 1989.

Deng, Z., Zhao, C., Zhang, Q., Huang, M., and Ma, X.: Statistical analysis of microphysical properties and the parameterization of effective radius of warm clouds in Beijing area, Atmospheric Research, 93, 888-896, 2009.

Derksen, J., Roelofs, G.-J., and Röckmann, T.: Influence of entrainment of CCN on microphysical properties of warm cumulus, Atmospheric chemistry and physics, 9, 6005-6015, 2009.

Desai, N., Liu, Y., Glienke, S., Shaw, R. A., Lu, C., Wang, J., and Gao, S.: Vertical Variation of Turbulent Entrainment Mixing Processes in Marine Stratocumulus Clouds Using High‐Resolution Digital Holography, Journal of Geophysical Research: Atmospheres, 126, e2020JD033527, 2021.

Freud, E., Rosenfeld, D., Andreae, M., Costa, A., and Artaxo, P.: Robust relations between CCN and the vertical evolution of cloud drop size distribution in deep convective clouds, Atmospheric Chemistry and Physics, 8, 1661-1675, 2008.

Freud, E., Rosenfeld, D., and Kulkarni, J. R.: Resolving both entrainment-mixing and number of activated CCN in deep convective clouds, Atmospheric Chemistry and Physics, 11, 12887-12900, 10.5194/acp-11-12887-2011, 2011.

Gao, W., Sui, C. H., Fan, J., Hu, Z., and Zhong, L.: A study of cloud microphysics and precipitation over the Tibetan Plateau by radar observations and cloud‐resolving model simulations, Journal of Geophysical Research Atmospheres, 121, 13,735-713,752, 2016.

Gao, Z., Liu, Y., Li, X., and Lu, C.: Investigation of turbulent entrainment‐mixing processes with a new particle‐resolved direct numerical simulation model, Journal of Geophysical Research: Atmospheres, 123, 2194-2214, 2018.

Gerber, H., Frick, G., Malinowski, S. P., Kumala, W., and Krueger, S.: POST—A new look at stratocumulus, American Meteorological Society 13th Conference on Cloud Physics, 2010.

Gerber, H., Frick, G., Malinowski, S. P., Jonsson, H., Khelif, D., and Krueger, S. K.: Entrainment rates and microphysics in POST stratocumulus, Journal of Geophysical Research: Atmospheres, 118, 12,094-012,109, 2013.

Gerber, H., Malinowski, S. P., and Jonsson, H.: Evaporative and radiative cooling in POST stratocumulus, Journal of the Atmospheric Sciences, 73, 3877-3884, 2016.

Gerber, H. E., Frick, G. M., Jensen, J. B., and Hudson, J. G.: Entrainment, mixing, and microphysics in trade-wind cumulus, Journal of the Meteorological Society of Japan. Ser. II, 86, 87-106, 2008.

Grabowski, W. W.: Indirect impact of atmospheric aerosols in idealized simulations of convective–radiative quasi equilibrium, Journal of climate, 19, 4664-4682, 10.1175/JCLI3857.1, 2006.

Haman, K. E., Malinowski, S. P., Kurowski, M. J., Gerber, H., and Brenguier, J.-L.: Small scale mixing processes at the top of a marine stratocumulus—a case study, Quarterly Journal of the Royal Meteorological Society, 133, 213-226, 10.1002/qj.5, 2007.

Hill, S. A., Krueger, S., Gerber, H., and Malinowski, S.: Entrainment interface layer of stratocumulus-topped boundary layers during POST, 13 AMS Conf. On Cloud Phys, 2010.

Hoffmann, F., and Feingold, G.: Entrainment and Mixing in Stratocumulus: Effects of a New Explicit Subgrid-Scale Scheme for Large-Eddy Simulations with Particle-Based Microphysics, Journal of the Atmospheric Sciences, 76, 1955-1973, 10.1175/jas-d-18-0318.1, 2019.

Hudson, James, G., Yum, Seong, and Soo: Droplet spectral broadening in marine stratus, Journal of the Atmospheric Sciences, 1997.

Jarecka, D., Grabowski, W. W., Morrison, H., and Pawlowska, H.: Homogeneity of the subgrid-scale turbulent mixing in large-eddy simulation of shallow convection, Journal of the atmospheric sciences, 70, 2751-2767, 2013.

Jen-La Plante, I., Ma, Y., Nurowska, K., Gerber, H., Khelif, D., Karpinska, K., Kopec, M. K., Kumala, W., and Malinowski, S. P.: Physics of Stratocumulus Top (POST): turbulence characteristics, Atmospheric Chemistry and Physics, 16, 9711, 2016.

Jensen, J., Austin, P., Baker, M., and Blyth, A.: Turbulent mixing, spectral evolution and dynamics in a warm cumulus cloud, Journal of the atmospheric sciences, 42, 173-192, 10.1175/1520-0469(1985)042<0173:TMSEAD>2.0.CO;2, 1985.

Jones, C., Bretherton, C., and Leon, D.: Coupled vs. decoupled boundary layers in VOCALS-REx, Atmospheric Chemistry and Physics, 11, 7143-7153, 2011.

Khain, A., Pinsky, M., and Magaritz‐Ronen, L.: Physical interpretation of mixing diagrams, Journal of Geophysical Research: Atmospheres, 123, 529-542, 2018.

Kumala, W., Haman, K., Kopec, M., Khelif, D., and Malinowski, S.: Modified ultrafast thermometer UFT-M and temperature measurements during Physics of Stratocumulus Top (POST), Atmospheric Measurement Techniques, 6, 2043-2054, 2013.

Kumar, B., Janetzko, F., Schumacher, J. R., and Shaw, R. A.: Extreme responses of a coupled scalar–particle system during turbulent mixing, New Journal of Physics, 14, 115020, 2012.

Kumar, B., Schumacher, J., and Shaw, R. A.: Cloud microphysical effects of turbulent mixing and entrainment, Theoretical and Computational Fluid Dynamics, 27, 361-376, 10.1007/s00162-012-0272-z, 2013.

Kumar, B., Götzfried, P., Suresh, N., Schumacher, J., and Shaw, R. A.: Scale Dependence of Cloud Microphysical Response to Turbulent Entrainment and Mixing, Journal of Advances in Modeling Earth Systems, 10, 2777-2785, 2018.

Lasher‐trapp, S. G., Cooper, W. A., and Blyth, A. M.: Broadening of droplet size distributions from entrainment and mixing in a cumulus cloud, Quarterly Journal of the Royal Meteorological Society: A journal of the atmospheric sciences, applied meteorology and physical oceanography, 131, 195-220, 10.1256/qj.03.199, 2005.

Lehmann, K., Siebert, H., and Shaw, R. A.: Homogeneous and Inhomogeneous Mixing in Cumulus Clouds: Dependence on Local Turbulence Structure, Journal of the Atmospheric Sciences, 66, 3641-3659, 10.1175/2009jas3012.1, 2009.

Liu, Y., Daum, P. H., Chai, S. K., and Liu, F.: Cloud parameterizations, cloud physics, and their connections: an overview, Brookhaven National Lab., Upton, NY (US), 2002.

Lu, C., Liu, Y., and Niu, S.: Examination of turbulent entrainment‐mixing mechanisms using a combined approach, Journal of Geophysical Research: Atmospheres, 116, 10.1029/2011JD015944, 2011.

Lu, C., Liu, Y., Niu, S., and Vogelmann, A. M.: Lateral entrainment rate in shallow cumuli: Dependence on dry air sources and probability density functions, Geophysical Research Letters, 39, 2012.

Lu, C., Liu, Y., and Niu, S.: A method for distinguishing and linking turbulent entrainment mixing and collision-coalescence in stratocumulus clouds, Chin. Sci. Bull., 58, 545-551, 2013a.

Lu, C., Liu, Y., Niu, S., Krueger, S., and Wagner, T.: Exploring parameterization for turbulent entrainment-mixing processes in clouds, Journal of Geophysical Research Atmospheres, 118, 185-194, 2013b.

Lu, C., Niu, S., Liu, Y., and Vogelmann, A. M.: Empirical relationship between entrainment rate and microphysics in cumulus clouds, Geophysical Research Letters, 40, 2333-2338, 10.1002/grl.50445, 2013c.

Lu, C., Liu, Y., and Niu, S.: Entrainment-mixing parameterization in shallow cumuli and effects of secondary mixing events, Science China Press, 2014a.

Lu, C., Liu, Y., Niu, S., and Endo, S.: Scale dependence of entrainment-mixing mechanisms in cumulus clouds, Journal of Geophysical Research: Atmospheres, 119, 13,877-813,890, 10.1002/2014jd022265, 2014b.

Lu, C., Liu, Y., Zhu, B., Yum, S. S., Krueger, S. K., Qiu, Y., Niu, S., and Luo, S.: On Which Microphysical Time Scales to Use in Studies of Entrainment‐Mixing Mechanisms in Clouds, Journal of Geophysical Research: Atmospheres, 123, 3740-3756, 2018.

Luo, S., Lu, C., Liu, Y., Bian, J., Gao, W., Li, J., Xu, X., Gao, S., Yang, S., and Guo, X.: Parameterizations of Entrainment‐Mixing Mechanisms and Their Effects on Cloud Droplet Spectral Width Based on Numerical Simulations, Journal of Geophysical Research: Atmospheres, 125, e2020JD032972, 2020.

Ma, Y.-F., Malinowski, S. P., Karpińska, K., Gerber, H. E., and Kumala, W.: Scaling analysis of temperature and liquid water content in the marine boundary layer clouds during POST, Journal of the Atmospheric Sciences, 74, 4075-4092, 2017.

Ma, Y. F., Pedersen, J., Grabowski, W., Kopec, M., and Malinowski, S.: Influences of Subsidence and Free‐Tropospheric Conditions on the Nocturnal Growth of Nonclassical Marine Stratocumulus, Journal of Advances in Modeling Earth Systems, 10, 2706-2730, 2018.

Malinowski, S. P., Haman, K., Kumula, W., Kopec, M., Gerber, H., and Krueger, S.: Smallscale variability of temperature and LWC at stratocumulus top, 13 AMS Conf. On Cloud Phys., th, 2010.

Malinowski, S. P., Gerber, H., Jen-La Plante, I., Kopec, M. K., Kumala, W., Nurowska, K., Chuang, P. Y., Khelif, D., and Haman, K. E.: Physics of Stratocumulus Top (POST): turbulent mixing across capping inversion, Atmospheric Chemistry and Physics, 13, 12171-12186, 2013.

Meischner, P., Baumann, R., and Holler, H.: Eddy Dissipation Rates in Thunderstorms Estimated by Doppler Radar in Relation to Aircraft In Situ Measurements, Journal of Atmospheric & Oceanic Technology, 18, 1609-1627, 2001.

Morrison, A. G.: Advanced Two-Moment Bulk Microphysics for Global Models. Part I: Off-Line Tests and Comparison with Other Schemes, Journal of Climate, 28, 1288-1307, 2015.

Panofsky, H. A.: Atmospheric turbulence, Models and methods for engineering applications., 397, 1984.

Pawlowska, H., Brenguier, J., and Burnet, F.: Microphysical properties of stratocumulus clouds, Atmospheric research, 55, 15-33, 10.1016/S0169-8095(00)00054-5, 2000.

Shupe, M., Persson, P., Brooks, I., Tjernström, M., Sedlar, J., Mauritsen, T., Sjogren, S., and Leck, C.: Cloud and boundary layer interactions over the Arctic sea ice in late summer, Atmospheric Chemistry and Physics, 13, 9379-9399, 2013.

Siebert, H., Franke, H., Lehmann, K., Maser, R., Saw, E. W., Schell, D., Shaw, R. A., and Wendisch, M.: Probing finescale dynamics and microphysics of clouds with helicopter-borne measurements, Bull. Amer. Meteor. Soc, 87, 1727-1738, 2006.

Small, J. D., Chuang, P. Y., and Jonsson, H. H.: Microphysical imprint of entrainment in warm cumulus, Tellus B: Chemical and Physical Meteorology, 65, 19922, 2013.

Stephens, G. L.: Cloud feedbacks in the climate system: A critical review, Journal of climate, 18, 237-273, 10.1175/JCLI-3243.1, 2005.

Stevens, B.: Cloud transitions and decoupling in shear‐free stratocumulus‐topped boundary layers, Geophysical research letters, 27, 2557-2560, 2000.

Su, C.-W., Krueger, S. K., McMurtry, P. A., and Austin, P. H.: Linear eddy modeling of droplet spectral evolution during entrainment and mixing in cumulus clouds, Atmospheric research, 47, 41-58, 10.1016/S0169-8095(98)00039-8, 1998.

Telford, J.: Clouds with turbulence; the role of entrainment, Atmospheric research, 40, 261-282, 10.1016/0169-8095(95)00038-0, 1996.

Telford, J. W., and Chai, S. K.: A new aspect of condensation theory, pure and applied geophysics, 118, 720-742, 10.1007/bf01593025, 1980.

Wang, J., Daum, P. H., Yum, S. S., Liu, Y., Senum, G. I., Lu, M.-L., Seinfeld, J. H., and Jonsson, H.: Observations of marine stratocumulus microphysics and implications for processes controlling droplet spectra: Results from the Marine Stratus/Stratocumulus Experiment, Journal of Geophysical Research, 114, 10.1029/2008jd011035, 2009.

Wang, Y.: Aerosol-Cloud Interactions from Urban, Regional, to Global Scales, Springer, 2015.

Wang, Y., Niu, S., Lv, J., Lu, C., Xu, X., Wang, Y., Ding, J., Zhang, H., Wang, T., and Kang, B.: A new method for distinguishing unactivated particles in cloud condensation nuclei (CCN) measurements: Implications for aerosol indirect effect evaluation,

545 Geophysical Research Letters, 2019.

546 Wood, R.: Stratocumulus clouds, Monthly Weather Review, 140, 2373-2423, 2012.

547 Wyngaard, J. C.: Turbulence in the Atmosphere, Cambridge University Press, 2010.

548 Xu, X., and Xue, H.: Impacts of free-tropospheric temperature and humidity on nocturnal nonprecipitating marine
549 stratocumulus, Journal of the Atmospheric Sciences, 72, 2853-2864, 2015.

550 Xu, X., Lu, C., Liu, Y., Gao, W., Wang, Y., Cheng, Y., Luo, S., and Weverberg, K. V.: Effects of Cloud Liquid‐Phase
551 Microphysical Processes in Mixed‐Phase Cumuli Over the Tibetan Plateau, Journal of Geophysical Research: Atmospheres,
552 125, 2020.

553 Xue, H., and Feingold, G.: Large-eddy simulations of trade wind cumuli: Investigation of aerosol indirect effects, Journal of
554 the Atmospheric Sciences, 63, 1605-1622, 10.1175/JAS3706.1, 2006.

555 Yau, M. K., and Rogers, R. R.: A short course in cloud physics, Elsevier, 1996.

556 Yeom, J. M., Yum, S. S., Liu, Y., and Lu, C.: A study on the entrainment and mixing process in the continental stratocumulus
557 clouds measured during the RACORO campaign, Atmospheric Research, 194, 89-99, 10.1016/j.atmosres.2017.04.028, 2017.

558 Yum, S. S., Wang, J., Liu, Y., Senum, G., Springston, S., McGraw, R., and Yeom, J. M.: Cloud microphysical relationships and
559 their implication on entrainment and mixing mechanism for the stratocumulus clouds measured during the VOCALS project,
560 Journal of Geophysical Research: Atmospheres, 120, 5047-5069, 10.1002/2014jd022802, 2015.

561 Zhang, Q., Quan, J., Tie, X., Huang, M., and Ma, X.: Impact of aerosol particles on cloud formation: Aircraft measurements
562 in China, Atmos. Environ, 45, 665-672, 2011.

563 Zhao, C., and Garrett, T. J.: Effects of Arctic haze on surface cloud radiative forcing, Geophysical Research Letters, 42, 557-
564 564, 2015.

565 Zheng, Y., and Rosenfeld, D.: Linear relation between convective cloud base height and updrafts and application to satellite
566 retrievals, Geophysical Research Letters, 42, 6485-6491, 2015.

567 Zheng, Y., Rosenfeld, D., and Li, Z.: Quantifying cloud base updraft speeds of marine stratocumulus from cloud top radiative
568 cooling, Geophysical Research Letters, 43, 11,407-411,413, 2016.

569 Zheng, Y., Rosenfeld, D., and Li, Z.: A more general paradigm for understanding the decoupling of stratocumulus‐topped
570 boundary layers: The importance of horizontal temperature advection, Geophysical Research Letters, 47, e2020GL087697,
571 2020.

572

573   **Table 1.** List of different methods determining adiabatic values

Number	Methods
1	LWC_a: calculated from the adiabatic growth from cloud base; n_a: maximum number concentration in each level; r_{va}: calculated by $r_{va} = \sqrt[3]{\dfrac{LWC_a}{\frac{4}{3}\pi\rho_L n_a}}$.
2	LWC_a: calculated from the adiabatic growth from cloud base; r_{va}: maximum volume mean radius in each level; n_a: calculated by $n_a = \dfrac{LWC_a}{\frac{4}{3}\pi\rho r_{va}^3}$.
3	LWC_a: maximum liquid water content in each level n_a: maximum number concentration in each level; r_{va}: calculated by $r_{va} = \sqrt[3]{\dfrac{LWC_a}{\frac{4}{3}\pi\rho n_a}}$.
4	LWC_a: maximum liquid water content in each level; r_{va}: maximum volume mean radius in each level; n_a: calculated by $n_a = \dfrac{LWC_a}{\frac{4}{3}\pi\rho r_{va}^3}$.
5	n_a: maximum number concentration in the interval; r_{va}: maximum volume mean radius in the interval; LWC_a: calculated by $LWC_a = \dfrac{4}{3}\pi\rho r_{va}^3 n_a$.

574
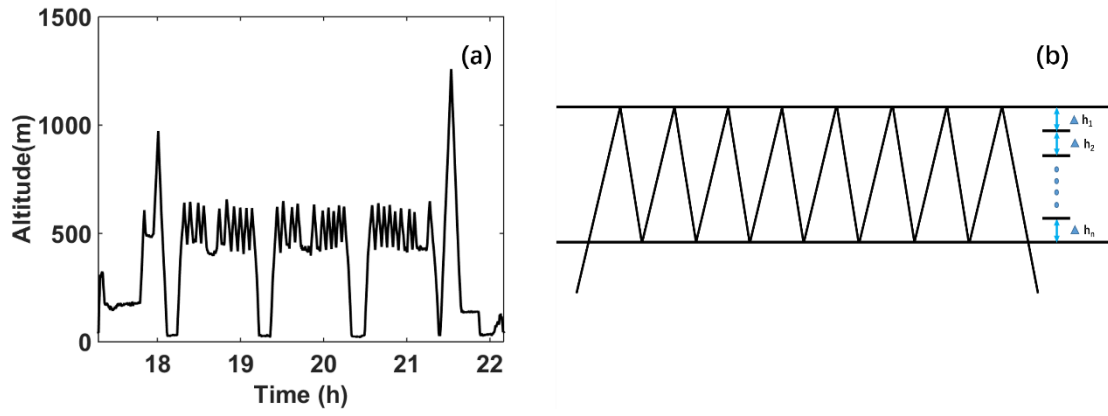
575

576   **Figure 1.** (a) Flight track on 16 July 2008. (b) Altitude stratification procedure of the sawtooth patterns, with the mean vertical resolution of

577   5 m such that $\Delta h_1 = \Delta h_2 = \cdots = \Delta h_n = 5$ m.
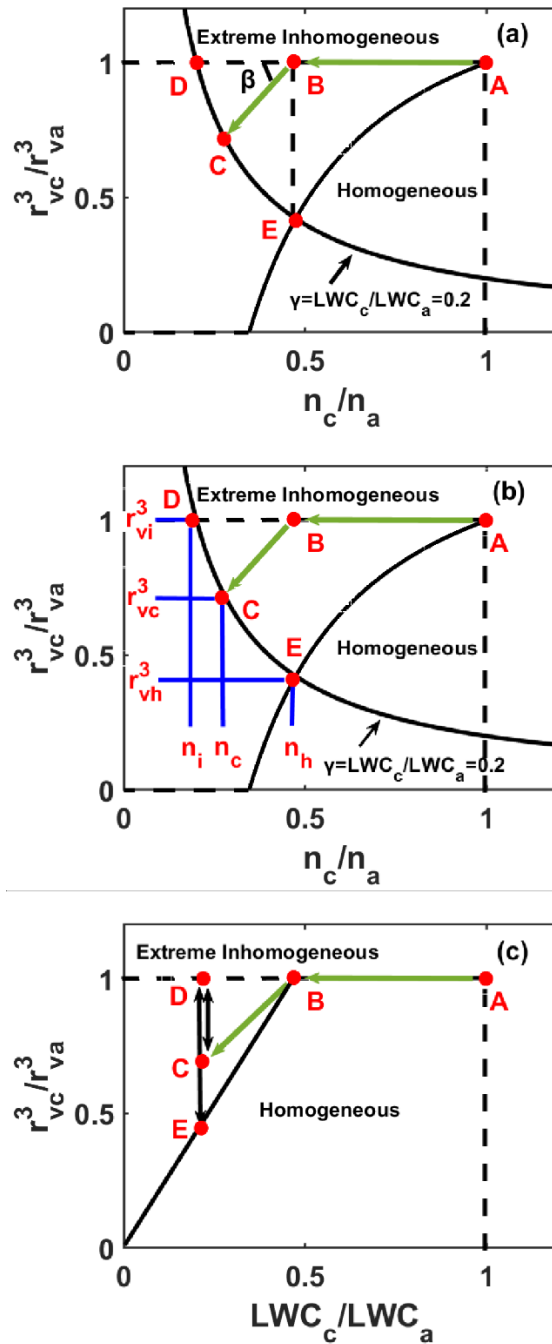
578

579 **Figure 2.** Microphysical diagram interpretating the definition for different homogeneous mixing degrees ((a) ψ_1; (b) ψ_2, ψ_3; (c) ψ_4). The

580 Points A and B represent the adiabatic state and the state after entrainment, respectively. If the extreme inhomogeneous mixing process

581 occurs, the cloud state approaches Point D; if the homogeneous mixing process occurs, the cloud state approaches Point E. The actual mixing

582 and evaporation processes are between the two extremes and cloud state approaches Point C. Extreme inhomogeneous mixing process is

583 represented by the horizontal dashed line; homogeneous mixing process is represented by the solid line starting from Point A in (a) and (b),

584 and the solid line starting from Point B in (c). Another black line in (a) and (b) corresponds to contour of $\gamma = 0.2$ defined as the ratio of liquid

585 water content (LWC$_c$) to its adiabatic value (LWC$_a$). See text for the meanings of other symbols.
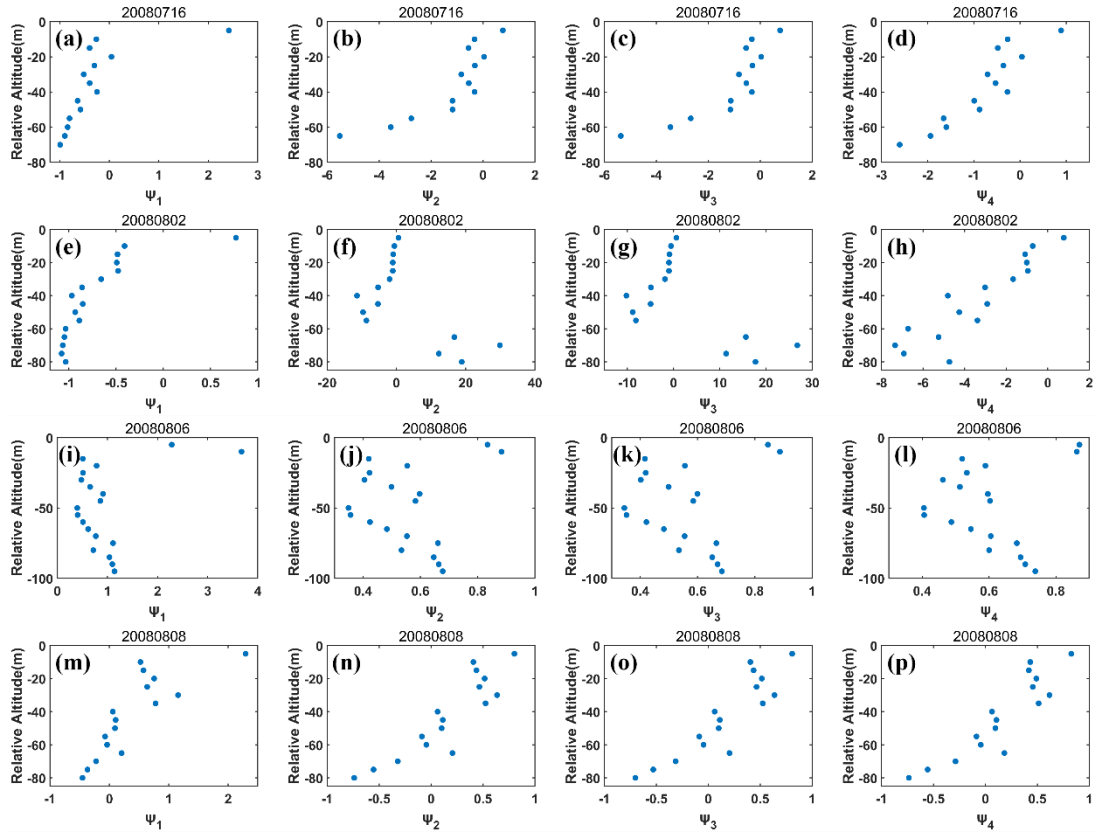
Figure 3. Height dependence of the first homogeneous mixing degree (ψ_1) on (a) 16 July 2008, (e) 02 August 2008, (i) 06 August 2008 and (m) 08 August 2008; height dependence of the second homogeneous mixing degree (ψ_2) on (b) 16 July 2008, (f) 02 August 2008, (j) 06 August 2008 and (n) 08 August 2008; height dependence of the third homogeneous mixing degree (ψ_3) on (c) 16 July 2008, (g) 02 August 2008, (k) 06 August 2008 and (o) 08 August 2008; and the fourth homogeneous mixing degree (ψ_4) on (d) 16 July 2008, (h) 02 August 2008, (l) 06 August 2008 and (p) 08 August 2008. The relative altitude on the y-axis equal to 0 represents the cloud tops. Adiabatic liquid water content (LWC$_a$) is obtained by the adiabatic growth from cloud base, adiabatic number concentration (n_a) is assumed to be the maximum volume mean radius at each level, and adiabatic volume mean radius (r_{va}) is calculated with LWC$_a$ and r_{va}.
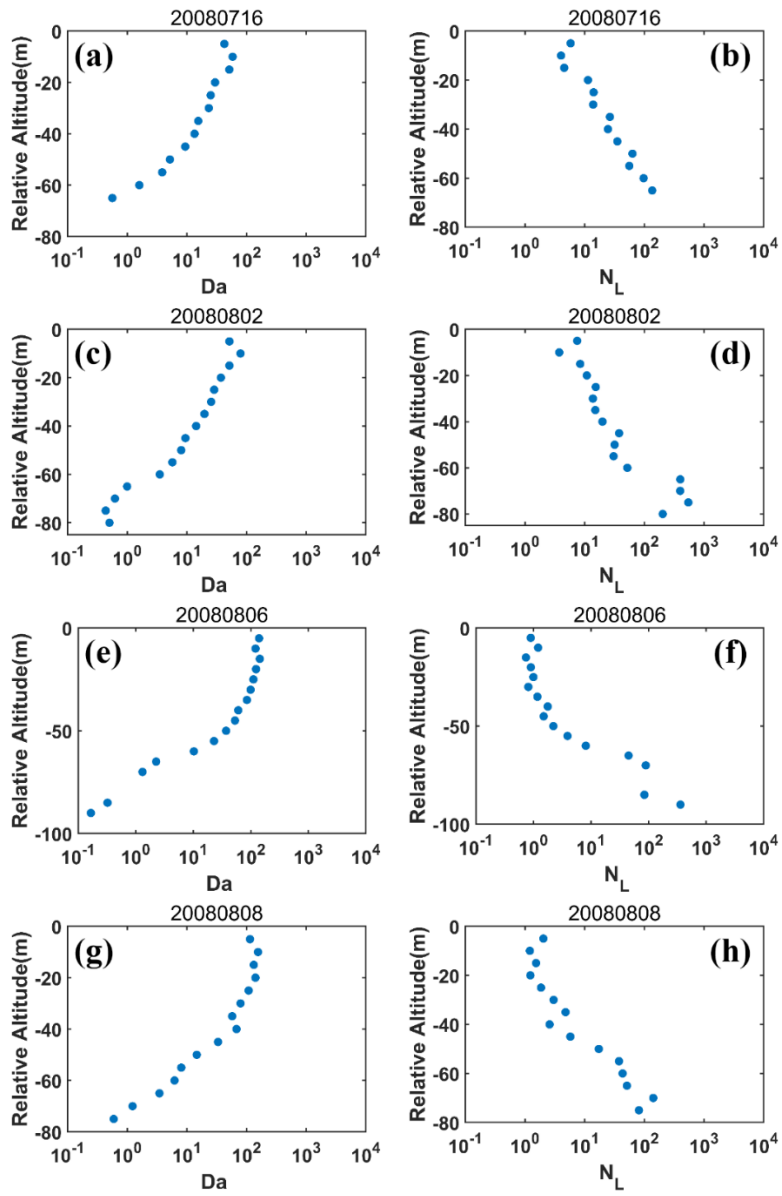
594

595 **Figure 4.** Height dependence of Damkohler number (*Da*) on (a) 16 July 2008, (c) 02 August 2008, (e) 06 August 2008 and (g) 08 August

596 2008; height dependence of transition scale number (N_L) on (b) 16 July 2008, (d) 02 August 2008, (f) 06 August 2008 and (h) 08 August

597 2008. The relative altitude on the y-axis equal to 0 represents the cloud tops. Adiabatic liquid water content (LWC$_a$) is obtained by the

598 adiabatic growth from cloud base, adiabatic number concentration (n_a) is assumed to be the maximum volume mean radius at each level,

599 and adiabatic volume mean radius (r_{va}) is calculated with LWC$_a$ and r_{va}.

600
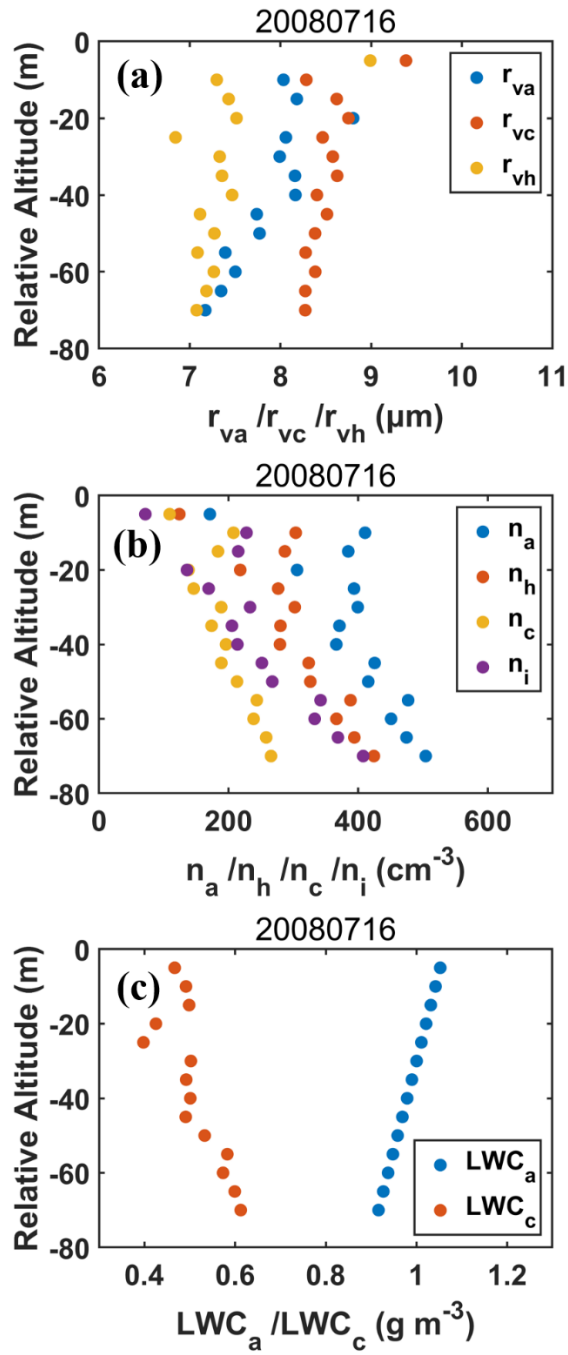
Figure 5. Height dependence of (a) r_{va}, r_{vc}, r_{vh}, (b) n_a, n_h, n_c, n_i and (c) LWC$_a$, LWC$_c$ on 16 July 2008. The relative altitude on the y-axis

equal to 0 represents the cloud tops. Adiabatic liquid water content (LWC$_a$) is obtained by the adiabatic growth from cloud base, the maximum

number concentration at each level is assumed to be adiabatic number concentration (n_a), and adiabatic volume radius (r_{va}) is calculated with

LWC$_a$ and n_a.

605
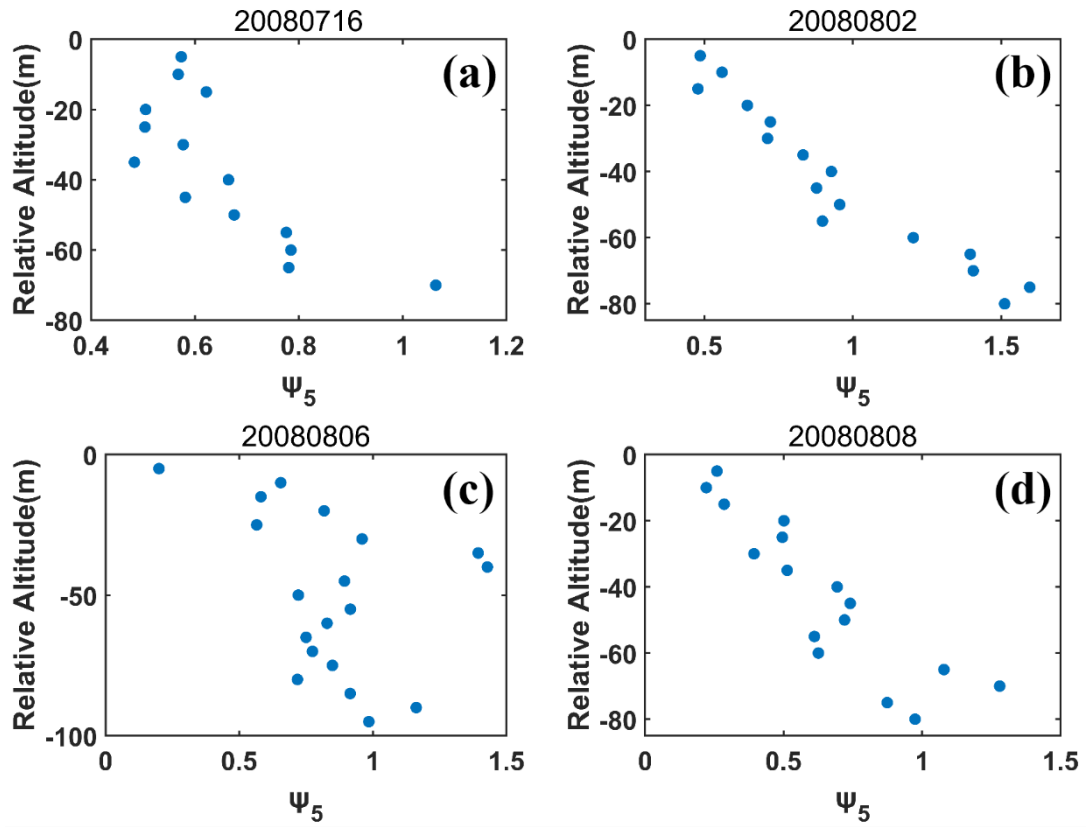
Figure 6. Height dependence of the newly defined homogeneous mixing degree (ψ_5) on (a) 16 July 2008, (b) 02 August 2008, (c) 06 August

2008 and (d) 08 August 2008. The relative altitude on the y-axis equal to 0 represents the cloud tops.

608

609
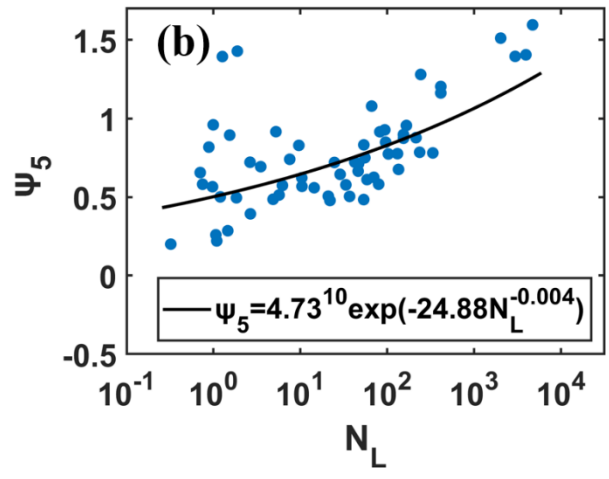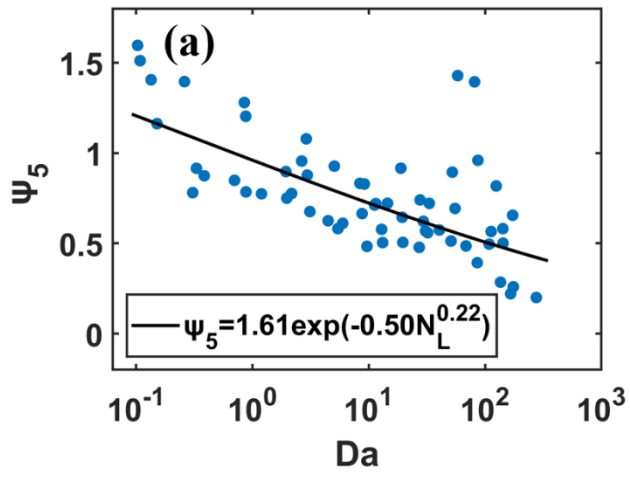
Figure 7. Relationships of the newly defined homogeneous mixing degree (ψ_5) versus (a) Damkohler number (Da) and (b) transition scale

number (N_L).

612
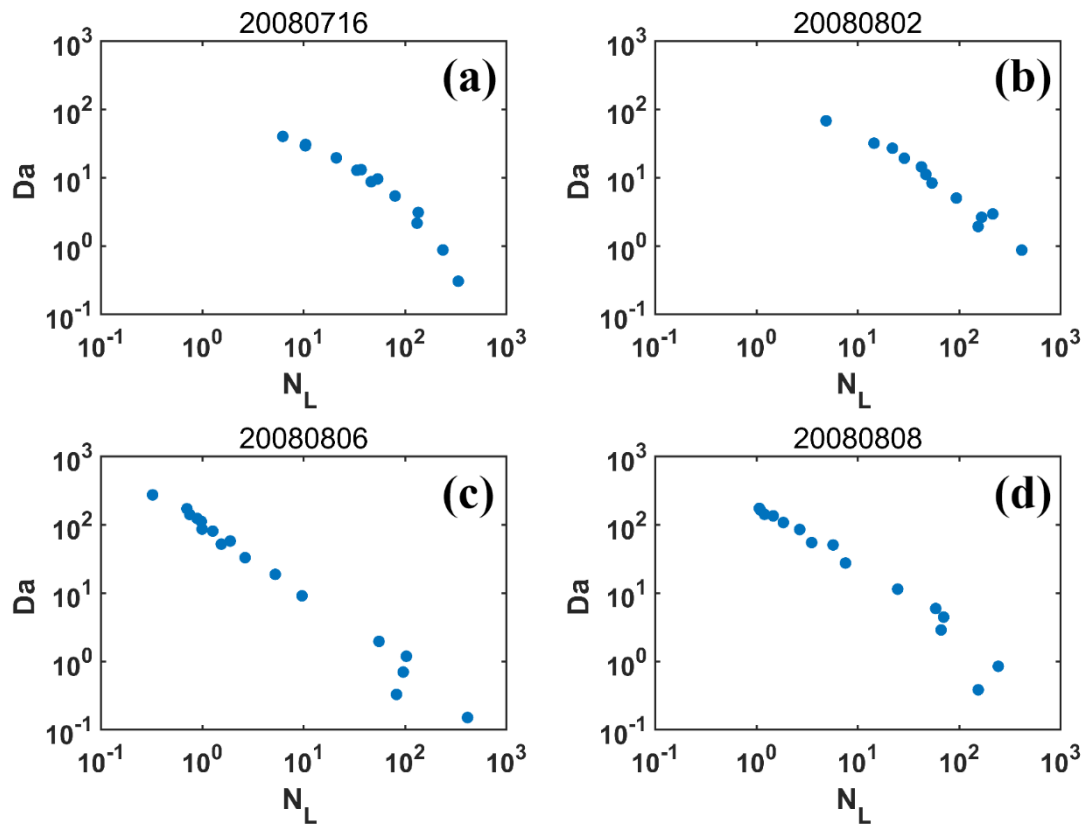
Figure 8. Relationships of Damkohler number (*Da*) versus transition scale number (N_L) on (a) 16 July 2008, (b) 02 August 2008, (c) 06

August 2008 and (d) 08 August 2008.

615
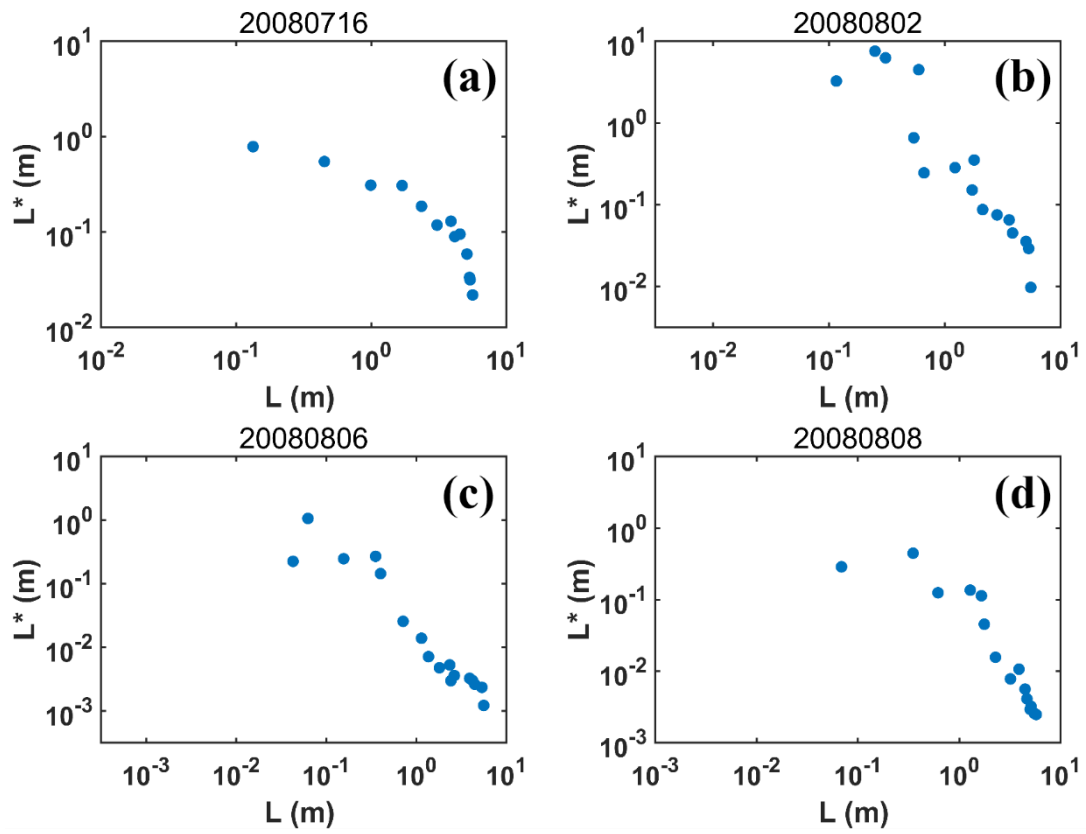
Figure 9. Relationships of transitional scale (L^*) versus droplet-free air length (L) on (a) 16 July 2008, (b) 02 August 2008, (c) 06 August 2008 and (d) 08 August 2008.
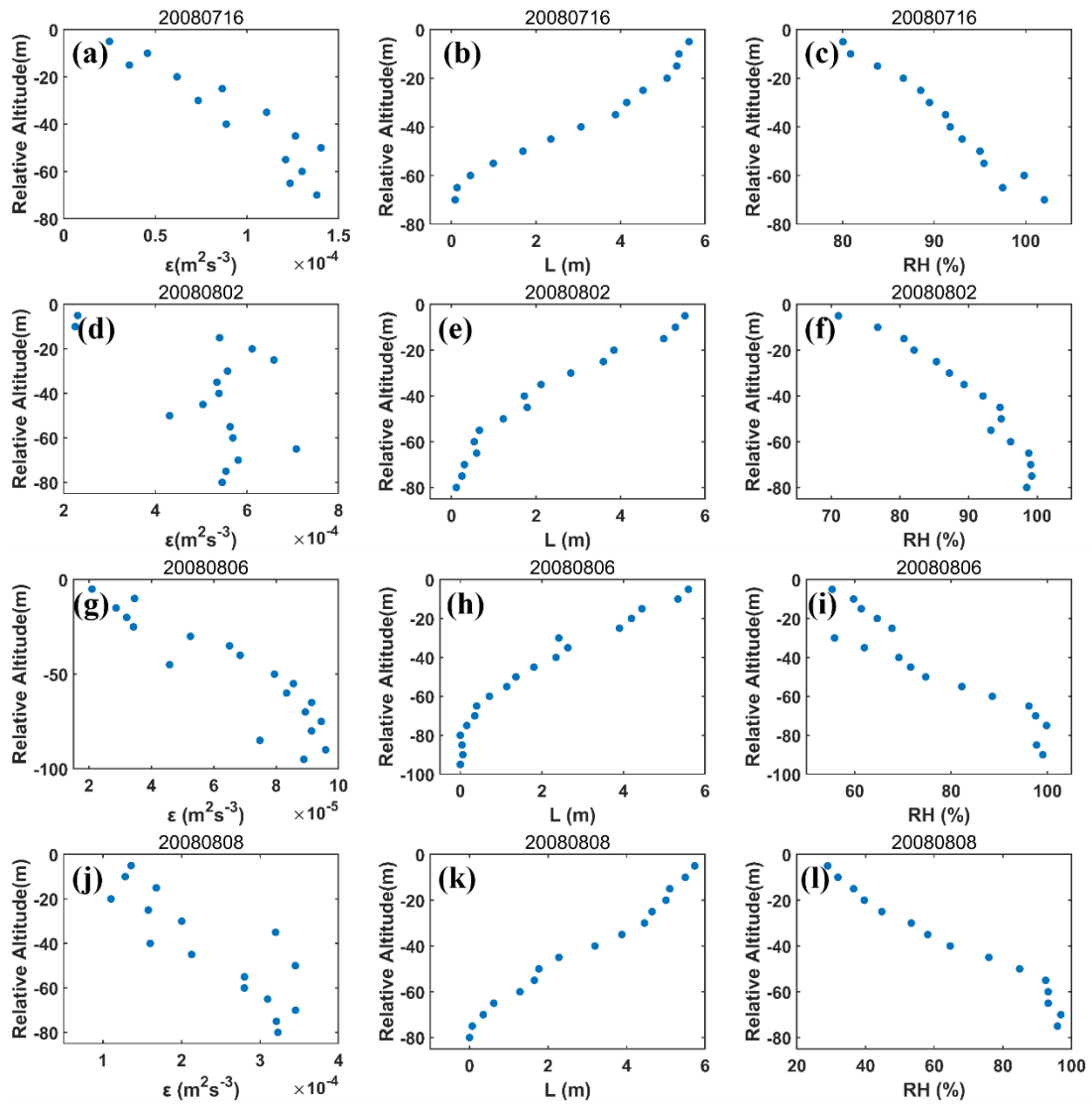
Figure 10. Height dependence of dissipation rate (ε) on (a) 16 July 2008, (d) 02 August 2008, (g) 06 August 2008 and (j) 08 August 2008; height dependence of relative humidity (RH) of droplet-free air on (b) 16 July 2008, (e) 02 August 2008, (h) 06 August 2008 and (k) 08 August 2008; and height dependence of length of droplet-free air (L) on (c) 16 July 2008, (f) 02 August 2008, (i) 06 August 2008 and (l) 08 August 2008. The relative altitude on the y-axis equal to 0 represents the cloud tops.